Author(s): Arnlund, David; Johansson, Linda C.; Wickstrand, Cecilia; Barty, Anton; Williams, Garth J.; Malmerberg, Erik; Davidsson, Jan; Milathianaki, Despina; DePonte, Daniel P.; Shoeman, Robert L.; Wang, Dingjie; James, Daniel; Katona, Gergely; Westenhoff, Sebastian; White, Thomas A.; Aquila, Andrew; Bari, Sadia; Berntsen, Peter; Bogan, Mike; van Driel, Tim Brandt; Doak, R. Bruce; Kjær, Kasper Skov;

Title: Visualizing a protein quake with time-resolved X-ray scattering at a free-electron laser

Year: 2014

Version: Accepted version (Final draft)

Visualizing a protein quake with time resolved X-ray scattering at a free electron laser

David Arnlund[1], Linda C. Johansson[1], Cecilia Wickstrand[1], Anton Barty[2], Garth J. Williams[3], Erik Malmerberg[1], Jan Davidsson[4], Despina Milathianaki[3], Daniel P. DePonte[2,3], Robert L. Shoeman[5,6], Dingjie Wang[7], Daniel James[7], Gergely Katona[1], Sebastian Westenhoff[1], Thomas A. White[2], Andrew Aquila[2], Sadia Bari[6,8], Peter Berntsen[1], Mike Bogan[9], Tim Brandt van Driel[10], R. Bruce Doak[5,7], Kasper Skov Kjær[10,11], Matthias Frank[12], Raimund Fromme[13], Ingo Grotjohann[13], Robert Henning[14], Mark S. Hunter[13], Richard A. Kirian[7], Irina Kosheleva[14], Christopher Kupitz[13], Mengning Liang[2], Andrew V. Martin[2], Martin Meedom Nielsen[10], Marc Messerschmidt[2,3], M. Marvin Seibert[3], Jennie Sjöhamn[1], Francesco Stellato[2], Uwe Weierstall[7], Nadia A. Zatsepin[7], John C. H. Spence[7], Petra Fromme[13], Ilme Schlichting[5,6], Sébastien Boutet[3], Gerrit Groenhof[15,16], Henry N. Chapman[2,17,18], Richard Neutze[1].

Corresponding author: richard.neutze@chem.gu.se

1. *Department of Chemistry and Molecular Biology, University of Gothenburg, Gothenburg, Sweden.*

2. *Center for Free-Electron Laser Science, Deutsches Elektronen-Synchrotron DESY, Hamburg, Germany.*

3. *Linac Coherent Light Source, Stanford Linear Accelerator Center (SLAC) National Accelerator Laboratory, Menlo Park, CA, USA.*

4. *Department of Photochemistry and Molecular Science, Uppsala University, Uppsala, Sweden.*

5. *Max-Planck-Institut für medizinische Forschung, Heidelberg, Germany.*

6. *Max Planck Advanced Study Group, Center for Free Electron Laser Science, Hamburg, Germany*.

7. *Department of Physics, Arizona State University, Tempe, Arizona, USA.*

8. *Max-Planck-Institut für Kernphysik, Heidelberg, Germany.*

9. *Photon Ultrafast Laser Science and Engineering Center Institute, Stanford Linear Accelerator Center (SLAC) National Accelerator Laboratory, Menlo Park, California, USA.*

10. *Department of Physics, Technical University of Denmark, Lyngby, Denmark.*

11. *Niels Bohr Institute, University of Copenhagen, Copenhagen, Denmark.*

12. *Lawrence Livermore National Laboratory, Livermore, California, USA.*

13. *Department of Chemistry and Biochemistry, Arizona State University, Tempe, Arizona, USA.*

14. *BioCARS, The University of Chicago, Illinois, USA.*

15. *Nanoscience Center, University of Jyväskylä, Jyväskylä, Finland.*

16. *Department of Chemistry, University of Jyväskylä, Jyväskylä, Finland.*

17. *Department of Physics, University of Hamburg, Hamburg, Germany.*

18. Centre for Ultrafast Imaging, Hamburg, Germany.

A 'protein quake' describes the hypothesis that proteins rapidly dissipate energy through quake like structural motions. Here we measure ultrafast structural changes in the *Blastochloris viridis* photosynthetic reaction center following multi-photon excitation using time-resolved wide angle X-ray scattering at an X-ray free electron laser. A global conformational change arises within picoseconds, which precedes the propagation of heat through the protein. This motion is damped within a hundred picoseconds.

Nature has evolved proteins to harvest both the energy and information content of light. Consequently, all light driven proteins share a common problem: how can the energy of an absorbed photon be usefully harvested without compromising the integrity of the protein when this energy is similar in magnitude to the protein's folding energy? Excess energy must be dissipated before irreversible damage occurs. The term 'protein quake' has been coined to describe how protein strain is released as a structural deformation that rapidly propagates away from a focus within the protein.[1,2] Results from time-resolved spectroscopy[3-6] have also suggested that the primary charge separation reactions of photosynthesis may be coupled to ultrafast protein structural changes. A deeper understanding of these phenomena requires experimental tools that directly probe protein conformational changes with picosecond time-resolution.

Time-resolved wide angle X-ray scattering (TR-WAXS) is a synchrotron based method that measures the nature and time-scale of global structural changes within proteins.[7-14] The time-resolution at these sources is limited to 100 ps due to the electron bunch duration within a storage ring. In contrast, X-ray free electron lasers (XFELs) deliver extremely brilliant X-ray pulses a few tens of femtoseconds in duration.[15] Here we use multi-photon excitation of the photosynthetic reaction center of *Blastochloris viridis* (RC$_{vir}$, **Supplementary Fig. 1**) to

demonstrate that TR-WAXS data recorded using XFEL radiation can capture an ultrafast protein conformational change that arises in picoseconds yet is rapidly damped.

Experiments were performed at the coherent X-ray imaging[16] (CXI) experimental station of the Linac Coherent Light Source[15] (LCLS) at SLAC National Accelerator Laboratory. Because of the extreme brilliance of XFEL radiation, for which 40 fs X-ray pulses containing 2.6×10^{12} photons/pulse were concentrated into a 10 μm^2 focal spot, we injected samples of detergent solubilized RC_{vir} across the XFEL beam using a gas focused liquid microjet[17] (**Fig. 1a**). The jet velocity was approximately 10 m s^{-1} and so samples were translated several cm between each X-ray pulse; every XFEL pulse therefore interacted with a fresh RC_{vir} sample and this avoided any build-up of laser or X-ray induced damage; both the XFEL repetition rate and the X-ray detector readout rate were 120 Hz and therefore WAXS data were recorded for each and every X-ray pulse; the 800 nm pump laser was operated at 60 Hz with dark and light images interleaved; the 800 nm laser path length through the microjet was ~ 10 μm giving a low sample optical density ($OD_{800 \, nm}$~ 0.04) and ensuring homogeneous excitation; and the vacuum sample chamber removed background from air scattering. The major disadvantages of this experimental geometry were instabilities in the microjet and X-ray detector which led to more data being rejected from statistical criteria than is typical for TR-WAXS studies at synchrotrons (Online Methods).

Samples were photoactivated using 800 nm optical pulses of 500 fs duration and a pulse fluence of 5.3 mJ mm^{-2}, which leads to considerable multi-photon absorption in RC_{vir} (approximately 800 photons per RC molecule, Online Methods). Bacteriochlorophyll cofactors are highly resilient to high fluence and thus, despite the energy absorbed by every RC_{vir} molecule being orders of magnitude above the activation energy of protein unfolding,[18]

photoexcited RC_{vir} molecules largely survived undamaged in control experiments at a similar pump laser fluence (**Supplementary Fig. 2**). X-ray images were integrated in rings and difference scattering amplitudes ($\Delta S(q, \Delta t)$, photoactivated minus dark) were calculated as a function of the time delay (Δt) between the optical laser and XFEL pulses (**Fig. 1b**).

TR-WAXS data (**Fig. 1b**) were separated into their major components by spectral decomposition,[8,11] which exploits differences in the rates of growth and decay of each component (**Fig. 1c**) to extract basis spectra (**Fig. 1d**). These data were described by a minimal set of four components: an ultrafast component (C1) that was set equal to $\Delta S(q,\Delta t)$ averaged over the first three time points after photoactivation; a protein component (C2) that displays oscillatory features characteristic of protein difference scattering[7-14] (**Supplementary Fig. 3**); and non-equilibrated (C3) and equilibrated (C4) heating components. Since the photoactivated sample volume is thermally homogeneous within 100 ps, but which precedes thermal expansion,[10] the equilibrated heating basis spectrum (C4) is almost identical to $\Delta S(q,\Delta t)$ averaged over the final three time-points. The temperature jump induced by the 800 nm pump laser was estimated to be 7 ℃ $\pm$ 1 ℃ by comparing $\Delta S(q,\Delta t)$ for the 280 ps time delay with temperature calibration WAXS curves measured using synchrotron radiation (**Supplementary Fig. 4**). All experimental data (**Fig. 3b**) were well approximated by a linear sum of the basis spectra C1 to C4 (**Fig. 3a**). Conversely, the time-dependence of the linear amplitudes of components C1 to C4 were well approximated by the modeled time-dependent amplitudes used to extract these basis spectra (**Supplementary Fig. 5**).

Molecular dynamics (MD) simulations of detergent solubilized RC_{vir} with 15,000 kJ mol^{-1} of energy deposited into the bacteriochlorophyll cofactors were used to characterize the flow of heat from the bacteriochlorophyll cofactors into, and out of, the protein. This impulse

instantaneously heated the cofactors by a few thousand Kelvin (**Fig. 2a**), which cooled by half within 7 ps as heat was dispersed into the surrounding protein, micelle and solvent. The time scale for when the heat content of the protein peaks as estimated by MD simulations (t_{max} = 14 ps, **Fig. 2b**) agrees strikingly well with the measured peak of the non-equilibrated heating component C3 (t_{max} = 14 ps, **Fig. 1c**, **Supplementary Fig. 5c**). Similarly, the time-dependence of the experimental equilibrated heating component C4 agrees with the flow of heat out of the protein and into the surrounding solvent as predicted from MD simulations (**Fig. 2b**). We therefore conclude that C3 and C4 measure the flow of heat through the protein and into the surrounding media, respectively, and can be experimentally distinguished due to contrast between the temperature dependence of the protein and solvent WAXS spectra. Accordingly, heat conduction dissipates the protein's kinetic energy within a few tens of picoseconds, orders of magnitude faster than the time-scale characteristic of protein unfolding.[7]

Basis spectra C1 and C2 describe the protein's structural dynamics. The growth of C1, which has $\Delta S(q)$ negative below $q \leq 0.3$ Å^{-1} but is otherwise featureless, was too rapid to be resolved (**Supplementary Fig. 5a**) and this component decayed by half within 3.2 ps. In contrast basis spectrum C2 contains oscillations in $\Delta S(q)$ between 0.2 Å$^{-1} \leq q \leq 0.9$ Å^{-1} (**Fig. 3b**), which are the fingerprint of protein structural changes as observed for bacteriorhodopsin on slower time-scales[8] (**Supplementary Fig. 3**). These oscillations are not observed in WAXS difference data recorded from continuously heated RC$_{vir}$ samples (**Supplementary Fig. 4a**) nor in TR-WAXS data recorded using synchrotron radiation (**Supplementary Fig. 4b**). We therefore conclude that C2 reveals an ultrafast protein conformational change that is half maximum Δt = 1.4 ps after photoactivation, peaks at Δt = 7 ps, and decays with a half-life of 44 ps. This

structural deformation propagates away from the epicenter of the protein quake in advance of thermal diffusion, preceding the flow of heat into the protein by approximately 2 ps (**Fig. 1c**).

TR-WAXS is directly sensitive to protein structure and several groups have modeled conformational changes against difference WAXS data.[8,9,11-14] Since no crystallographic structures exist to guide structural modeling on an ultrafast time-scale, we compared predictions recovered from photoexcited and reference MD simulations of RC_{vir} against the ultrafast (C1) and protein (C2) difference WAXS basis spectra. This approach guarantees that all sampled structures are chemically accessible from the resting RC_{vir} structure within a few ps after thermal energy is deposited into the protein's co-factors. Since heat is initially contained within the light-absorbing cofactors (**Fig. 2**), we performed χ^2 fitting[11] (Online Methods) to C1 by considering only motions of the bacteriochlorophyll cofactors, with the rest of the protein artificially frozen. The change in WAXS spectra predicted from a selected ensemble of 720 structural pairs is compatible with the C1 basis spectrum (**Fig. 3a**). For χ^2 fitting to C2 we allowed motions of the entire protein and the WAXS changes predicted from the ensemble average of 720 selected structural pairs reproduces all major features of the difference WAXS basis spectrum (**Fig. 3b**).

Recurring movements were identified by calculating changes in the internal distance matrix on C_α atoms of photoexcited versus reference structures, $[\Delta \mathbf{C}_\alpha]_{ij}$, averaging this matrix over an ensemble set identified by χ^2 fitting, determining the standard deviation of this matrix over this ensemble set and examining the ratio of the average perturbation relative to its standard deviation (**Supplementary Fig. 6**). All recurring internal distance changes selected by this analysis (Online Methods, **Supplementary Fig. 6**) correspond to an increase of the internal distances between the C_α atoms of the protein's TM domains (**Fig. 3c**, **Supplementary Video**

1) and no recurrent movements of C_α atoms towards each other were identified. This shift in the ensemble average amounts to a modest (up to 1 Å in amplitude) expansion of the RC_{vir} TM domain (**Supplementary Video 2**).

These data and its analysis establish that XFEL radiation facilitates the direct visualization of ultrafast protein motions using TR-WAXS. While acknowledging that our use of multi-photon excitation is far removed from physiological conditions, these X-ray snapshots of a 'protein quake' nonetheless show that strain created by energy input into the RC_{vir} cofactors is relieved via a structural deformation that propagates through the protein more rapidly than heat. More experiments are needed to determine if similar motions are induced under physiological conditions of single-photon absorption. One interesting future application of XFEL based TR-WAXS is to search for phase coherent nuclear motions in photosynthetic reaction centers.[3] Ultrafast motions may also be functionally important in other energy transducing proteins such as photosystems I and II, light harvesting complexes and bacterial rhodopsins;[8,11] sensory receptors such as visual rhodopsin, sensory rhodopsin, photoactive yellow protein[12] and phytochromes;[14] or model heme containing proteins such as myoglobin[9,10] and hemoglobin.[7,13] Generic approaches that directly excite low-frequency normal-modes in proteins[2,19] using short pulsed THz lasers[20] will also facilitate ultrafast TR-WAXS studies at XFELs that explore the rise and decay of global motions in any protein or macromolecular assembly of choice.

ONLINE METHODS

Methods and any associated references are available in the online version of the paper at http://www.nature.com/naturemethods/.

Note: Supplementary information is available on the Nature Methods website.

Supplementary Information.

Online Methods.

Supplementary Figs. 1 to 6.

Supplementary Videos 1 and 2.

AUTHOR CONTRIBUTIONS

R.N. and D.A. conceived the experiment which was designed with E.M., J.D., A.B., H.N.C., J.C.H.S., S.Bo., G.W., D.d.P., R.B.D. and U.W.. Samples were prepared by D.A. and L.C.J.; Time resolved WAXS experiments at the LCLS were performed by D.A., L.C.J., A.B., G.W., C.W., E.M., J.D., D.M., D.d.P., R.L.S., D.W., D.J., G.K., S.W., T.A.W., A.A., S.Ba., M.B., R.B.D., M.F., R.F., I.G., M.S.H., R.A.K., C.K., M.L., A.V.M., M.M., M.M.S., J.S., F.S., U.Q., N.A.Z., P.F., I.S., S.Bo., H.N.C. and R.N. Time resolved WAXS experiments at Argonne National Laboratory were performed by D.A., L.C.J., P.B., J.S., J.D., R.H. and I.K.. The CXI instrument was setup by S.Bo., G.J.W., M.M. and M.M.S and the online fs laser was setup by D.M., J.D. and M.F.. Samples were delivered by R.L.S., S.Ba., D.d.P., U.W. and R.B.D. Data were analyzed by D.A., A.B., E.M. and C.W. Molecular dynamics simulations of RC_{vir} were performed by G.G., theoretical fitting by D.A. and C.W., and heat flow dynamics examined by G.G. K.S.K., T.v.D. and M.M.N. The manuscript was prepared by R.N., D.A. and G.G. with input from all authors.

COMPETING FINANCIAL INTERESTS

The authors declare no competing financial interests.

REFERENCES

1   Ansari, A. *et al.* Protein states and proteinquakes. *Proc. Natl. Acad. Sci. USA* **82**, 5000-5004 (1985).

2   Miyashita, O., Onuchic, J. N. & Wolynes, P. G. Nonlinear elasticity, proteinquakes, and the energy landscapes of functional transitions in proteins. *Proc. Natl. Acad. Sci. USA* **100**, 12570-12575 (2003).

3   Vos, M. H., Rappaport, F., Lambry, J.-C., Breton, J. & Martin, J.-L. Visualization of coherent nuclear motion in a membrane protein by femtosecond spectroscopy. *Nature* **363**, 320 - 325 (1993).

4   Rischel, C. *et al.* Low frequency vibrational modes in proteins: changes induced by point-mutations in the protein-cofactor matrix of bacterial reaction centers. *Proc. Natl. Acad. Sci. USA* **95**, 12306-12311 (1998).

5   Wang, H. *et al.* Protein dynamics control the kinetics of initial electron transfer in photosynthesis. *Science* **316**, 747-750 (2007).

6   Wang, H. *et al.* Unusual temperature dependence of photosynthetic electron transfer due to protein dynamics. *J. Phys. Chem. B* **113**, 818-824 (2009).

7   Cammarata, M. *et al.* Tracking the structural dynamics of proteins in solution using time-resolved wide-angle X-ray scattering. *Nat. Meth.* **5**, 881-886 (2008).

8   Andersson, M. *et al.* Structural dynamics of light-driven proton pumps. *Structure* **17**, 1265-1275 (2009).

9   Ahn, S., Kim, K. H., Kim, Y., Kim, J. & Ihee, H. Protein tertiary structural changes visualized by time-resolved X-ray solution scattering. *J. Phys. Chem. B* **113**, 13131-13133 (2009).

10   Cho, H. S. *et al.* Protein structural dynamics in solution unveiled via 100-ps time-resolved x-ray scattering. *Proc. Natl. Acad. Sci. USA* **107**, 7281-7286 (2010).

11   Malmerberg, E. *et al.* Time-resolved WAXS reveals accelerated conformational changes in iodoretinal-substituted proteorhodopsin. *Biophys. J.* **101**, 1345-1353 (2011).

12   Ramachandran, P. L. *et al.* The short-lived signaling state of the photoactive yellow protein photoreceptor revealed by combined structural probes. *J. Am. Chem. Soc.* **133**, 9395-9404 (2011).

13   Kim, K. H. *et al.* Direct Observation of Cooperative Protein Structural Dynamics of Homodimeric Hemoglobin from 100 ps to 10 ms with Pump-Probe X-ray Solution Scattering. *J Am. Chem. Soc.* **134**, 7001-7008 (2012).

14   Takala, H. *et al.* Signal amplification and transduction in phytochrome photosensors. *Nature* **509**, 245-248 (2014).

15   Emma, P. *et al.* First lasing and operation of an angstrom-wavelength free-electron laser. *Nat. Photon.* **4**, 641-647 (2010).

16   Boutet, S. & Williams, G. W. The Coherent X-ray Imaging (CXI) instrument at the Linac Coherent Light Source (LCLS). *New J. Phys.* **12**, 035024 (2010).

17   Weierstall, U., Spence, J. C. & Doak, R. B. Injector for scattering measurements on fully solvated biospecies. *Rev. Sci. Instrum.* **83**, 035108 (2012).

18   Palazzo, G., Lopez, F. & Mallardi, A. Effect of detergent concentration on the thermal stability of a membrane protein: The case study of bacterial reaction center solubilized by N,N-dimethyldodecylamine-N-oxide. *Biochim. Biophys. Acta* **1804**, 137-146 (2010).

19   Go, N., Noguti, T. & Nishikawa, T. Dynamics of a small globular protein in terms of low-frequency vibrational modes. *Proc. Natl. Acad. Sci. USA* **80**, 3696-3700 (1983).

20   Cook, D. J. & Hochstrasser, R. M. Intense terahertz pulses by four-wave rectification in air. *Opt. Lett.* **25**, 1210-1212 (2000).

CAPTIONS TO FIGURES:

Figure 1: Time dependent changes in WAXS data recorded from detergent solubilized samples of RC$_{vir}$. (**a**) Schematic of the experimental setup illustrating the microjet of solubilized RC$_{vir}$, X-ray detector, XFEL beam and the 800 nm pump laser. (**b**) Time-resolved WAXS difference data, $\Delta S(q, \Delta t) = S_{light}(q, \Delta t) - S_{dark}(q)$, recorded as a function of the time delay between the arrival of the 800 nm pump laser and the XFEL probe for 15 of 41 measured time delays. Linear sums of the four basis spectra (red) shown in **d** are superimposed upon the experimental difference data (black). (**c**) Time-dependent amplitudes of the components C1 to C4 used to extract the basis spectra. (**d**) Basis spectra extracted from the experimental data by spectral decomposition: C1, an ultrafast component (green); C2, a protein component (blue); C3, non-equilibrated (black) and C4, equilibrated (magenta) heating components.

Figure 2: MD simulations of the flow of heat throughout the system. (**a**) Temperature of the cofactors (dark and light blue, bacteriochlorophylls; red, special pair), protein (yellow), detergent micelle (purple), surrounding solvent (grey) and total system (black) determined from MD trajectories. (**b**) Heat content of the cofactors (red), protein (yellow), detergent micelle (purple) and solvent (grey). The experimental amplitudes of the non-equilibrated heating (C3, light blue) and equilibrated heating (C4, dark blue) basis spectra are scaled to aid comparison with the heat content of the protein and solvent extracted from MD simulations.

Figure 3: Structural analysis of the protein conformational changes. (**a**) Theoretical WAXS changes (red) predicted from χ^2 fitting to the ultrafast basis spectrum (C1, black) where only movements of the RC$_{vir}$ cofactors were considered. (**b**) Theoretical WAXS changes (red)

predicted from χ^2 fitting to the protein basis spectrum (C2, black) where RC_{vir} protein and cofactor atoms were allowed to move. (**c**) Stereo representation of light induced movements in RC_{vir}. Large spheres represent C_α atoms that display recurrent movements within an ensemble of structural changes selected by χ^2 fitting to C2 (**Supplementary Fig. 6**). Orange spheres represent C_α atoms with recurring movements away from other C_α atoms. No recurrent movements of C_α atoms towards other C_α atoms were identified. Cofactors are shown in grey.

ONLINE METHODS

Protein Production and Purification

Bl. viridis cells were cultured in 10 l glass bottles. After two days of room temperature incubation in the dark, bottles were illuminated for two days at 30 °C and harvested using a JLA-8.1000 rotor at 8000 x g for 10 minutes. Approximately 30 g of cells were retrieved from 10 l of culture. Cell membrane was extracted through sonication, after which the membrane was pelleted by centrifugation at $45000 \times g$ for 45 minutes. Membrane concentration was adjusted to $OD_{1012} = 100$ and solubilized in 4 % lauryldimethylamine-N-oxide (LDAO) for 3 h at room temperature. Unsolubilized membrane was pelleted by centrifugation at $45000 \times g$ for 75 minutes. Supernatant was transferred to a 250 ml POROS 50 micron HQ ion exchange media and fractions with A_{280}/A_{830} ratio of ≤ 4 were pooled, concentrated to 10 ml using a 100 000 MWCO concentration tube and then loaded on a HiPrep 26/60 Sephacryl S-300 column. Fractions with A_{280}/A_{830} ratio of ≤ 2.6 were pooled, concentrated to 30 mg ml^{-1} and flash-frozen for long term storage.

Data collection

Solubilized samples of RC$_{vir}$ were injected using a HPLC driven microjet[17,21] with a nozzle diameter of 50 μm, a flow rate of 10 μl min^{-1}, and achieving a jet diameter of 10 μm due to focusing by an outer stream of helium gas. The 800 nm fundamental of a Ti:Sa femtosecond laser was used to pump the sample using a pulse duration of 500 fs and pulse power of 260 μJ per pulse focused to a spot diameter for $I/I_0 = e^{-2}$ of 250 μm ± 25 μm. The selection of 500 fs pump pulse duration set the maximum temporal resolution accessible in this experiment. The pump laser had a Gaussian beam profile, with the average energy passing through the 250 μm circular focus corresponds to a fluence of 5.3 mJ mm^{-2}.

Data were collected at the Coherent X-ray Imaging instrument[16] (CXI) at the LCLS[15] in January 2012. The XFEL pulse repetition rate and the detector readout rate were both 120 Hz, with a new image being recorded after every X-ray exposure. The Ti:Sa laser was run with a repetition rate of 60 Hz such that light (laser on) and dark (laser off) images were interleaved. Diffraction data were recorded on a Cornell-SLAC Pixel Array Detectors (CSPAD).[22] The detector was built-up by 64 individual tiles with a pixel size of 110×110 μm^2, each tile consisting of 192×185 pixels. The sample to detector distance was 107 mm and data were collected from q = 0.1 Å^{-1} to 2.5 Å^{-1}.

The XFEL beam was tuned to 6 keV (wavelength 2.07 Å), focused to a spot size of 10 μm^2 and aligned to intersect the liquid jet before the Rayleigh breakup. Spatial overlap of the XFEL and Ti:Sa laser beams on the microjet was aided by observing an X-ray induced fluorescence of the sample from the liquid jet. The flow rate of the microjet was ~10 m s^{-1} which ensured that every X-ray pulse sampled a completely fresh sample, thereby avoiding all issues concerning 800 nm laser or XFEL induced accumulated damage to the sample. A preliminary analysis of the TR-WAXS data implemented during the experiment allowed the difference signal, $\Delta S(q, \Delta t)$, to be displayed approximately two minutes after data were collected. From this difference signal the temporal overlap was set ($\Delta t = 0 \pm 0.5$ ps) at the precise location of the microjet. The experimental necessity (at the time) to use $\Delta S(q)$ to establish $\Delta t = 0$ motivated our choice of a high pump laser fluence in these experiments.

Sample heating

The temperature jump induced by the pump laser within the sample volume under these conditions was 7 ± 1 ºC and was determined by comparison of the change in X-ray scattering in these experiments for $\Delta t = 280$ ps over the domain $1.0 \leq q \leq 2.5$ Å^{-1} against standard

heating curves recorded using synchrotron data[10] (**Supplementary Fig. 4a**). Because of shot-to-shot fluctuations in background in the XFEL data, the temperature calibration curves recorded using synchrotron data were first interpolated in 1 ºC steps over the temperature domain 0 ºC $\leq \Delta T \leq$ 20 ºC and 500 random numbers were then added to generate an ensemble of mock temperature measurements with random background fluctuations. The closest agreement to the XFEL data was for $\Delta T = 7$ ºC (**Supplementary Fig. 4c**). The time-resolved data recorded using synchrotron radiation established that $\Delta S(q, \Delta t = 280$ ps$) \approx \Delta S(q, \Delta t = 1$ µs) (**Supplementary Fig. 4b**) which justifies this calibration, since the sample is fully expanded and in thermal equilibrium for $\Delta t = 1$ µs[10,23] and can therefore be compared against standard temperature calibration curves.

A temperature jump of $\Delta T = 7 \pm 1$ ºC corresponds to 800 ± 100 photons absorbed per RC_{vir} molecule within the sampled volume, which is far removed from normal physiological conditions. The RC_{vir} molar extinction coefficient[24] is high at 800 nm ($\varepsilon_{800\,nm} \sim 1.8 \times 10^5 \pm 0.2 \times 10^5$ M^{-1} cm^{-1}) such that, assuming an incident laser fluence of 5.3 mJ mm^{-2}, approximately 800 photons would be absorbed per RC_{vir} molecule if 55 % of the incident light were scattered from the microjet. In reality the photochemistry is more complex since high photon-flux densities cause exciton annihilation[25,26] resulting in one electronically deexcited and one highly excited species. Moreover, highly excited species undergo rapid radiationless relaxation into vibrational modes according to Kasha's rule[27] and it is very difficult to reach high lying electronic states because the more excited the molecule becomes the more rapidly it decays through vibrational coupling.

Data analysis

Radially integrated stacks of each run were extracted using Cheetah software (https://github.com/antonbarty/cheetah) and difference scattering curves were obtained using MatLab. Radially integrated data were normalized between q = 2.10 to 2.20 Å^{-1}. Three 3σ criteria rejection routines were performed on this data: an initial rejection on the absolute scattering data; a second rejection on the normalized data; and a final rejection on the difference curves. Approximately 9000 differences measurements were thus merged for each time point representing approximately 60 % of all recorded data, which is a smaller fraction than typically kept when using synchrotron radiation (~ 95 %).

A total of 41 difference WAXS traces, $\Delta S(q,\Delta t)$, for 41 different time-delays, Δt, between the arrival of the 800 nm optical laser and X-ray laser pulses, were processed by spectral decomposition.[8] Spectral decomposition is similar to principle component analysis but specifies the time-dependence of the states to be extracted according to a kinetics scheme (**Fig. 1c**). Four components were extracted from the data (**Fig. 1d**): an ultrafast component (C1); a second component identified as due to protein conformational changes (C2); and two heating components: non-equilibrated (C3) and equilibrated (C4). All components were modeled as simple first-order kinetics (exponential rise and decay) with the decay of the C3 heating component being coupled to the growth of the C4 heating component (*ie*. C3 → C4) and a time offset of approximately 2 ps was needed to fit the rise of C3. We initially focused on the time-dependence of WAXS differences within the domain q = 1.35 to 2.5 Å^{-1} so as to extract the time-dependence of the components C3 and C4; and $\Delta S(q)$ averaged over the first three time points was used to define C1. Iterative cycles of subtracting the C3, C4 and C1 basis spectra from the WAXS data so as to characterize the C2 component; followed by removing the C2 component from all data so as to better characterize the C3 and C4 basis spectra; yielded the optimal basis spectra (**Fig. 1d**). All four components were used to

reproduce the entire data set as a linear sum of these components (**Fig. 1b**) and to validate the kinetic model used for spectral decomposition (Supplementary **Fig. 5**).

On the picosecond time-scale it might be expected that a description of these data in terms of four time-independent functions (C1(q) to C4(q)) with time-dependent amplitudes may break down since a localized perturbation in real space corresponds to a delocalized response in q space that evolves in time. This simple description, however, proved to be satisfactory given the errors within this experimental data (**Fig. 1b**) although future analysis of TR-WAXS studies of ultrafast protein dynamics may require modifications to this scheme.

Synchrotron based data collection

Difference WAXS data for both steady-state heating (Supplementary **Fig. 4a**) and for the time-points Δt = 280 ps and 1 μs (Supplementary **Fig. 4b**) were recorded at the Advanced Photon Source of Argonne National Laboratory (APS) using the setup as described.[10] Steady state measurements used an Oxford cryostream to heat the sample as it flowed through a capillary; and time-resolved WAXS measurements used 100 ps X-ray pulses isolated using a microsecond chopper[28] and a 780 nm picosecond laser to excite the sample.

Molecular Dynamics Simulations

Reaction center coordinates were taken from the 2.3 Å X-ray structure of detergent solubilized RC$_{vir}$[29] (pdb entry 1PRC). All interactions were modeled with the Amber03 force field[30]. Bonded and Lennard-Jones parameters used to model the co-factors bacteriochlorophyll B, bacteriophytin B, menaquinone and ubiquinone, were taken from Cecarelli and co-workers[31], who derived the these parameters for bacteriochlorophyll A, bacteriophytin A and ubiquinone, the cofactors in the reaction center of *R. sphaeroides*

(RC$_{sph}$). Because the same atom types occur in the cofactors in RC$_{sph}$ and RC$_{vir}$, we constructed new force fields for bacteriochlorophyll B, bacteriophytin B and menaquinone based on the atomtype information provided by Cecarelli et al.[31]. Partial charges were rederived for all atoms of the co-factors, following Amber03 charge parameterization philosophy[30]. The structures of the isolated co-factors, without their aliphatic tails (for which the default Amber03 charges were used) were minimized at the HF/6-31G** level of *ab initio* theory. To include the effect of the protein environment in these calculations, the IEFPCM continuum solvent model was used with a relative dielectric of 4. After geometry optimization, the electrostatic potential at 10 concentric layers of 17 points per unit area around each atom was evaluated using the electron density calculated at the B3LYP/cc-pVTZ level of theory, again using the IEFPCM continuum solvent model with a relative dielectric of 4. The atomic charges were obtained by performing a two stage RESP fit to the electrostatic potential. The force field parameters for the Heme(III) co-factors were taken from Authenrieth and co-workers[32] without modifications. Gromacs topology files and starting coordinates are available for download from wwwuser.gwdg.de/~ggroenh/RC_vir.tar.gz.

The RC$_{vir}$ structure was minimized in vacuum using infinite cut-offs for both Lennard-Jones and Coulomb interactions. After minimization, the protein complex was embedded into a micelle that was composed of LDAO detergent molecules. Following the estimates of Gast *et al.*[33], 260 detergent molecules were used to solvate the TM portion of the protein. After insertion, around 187 Na$^+$ and 188 Cl$^-$ ions were added to the water phase to create a 0.2 M salt solution. The total system contained 145,368 atoms and was equilibrated for 20 ns with harmonic position restraints on the heavy protein and co-factor atoms (force-constant 1000 kJmol^{-1}nm^{-2}). After releasing these restraints, the system was further equilibrated for 14 ns.

Equilibration simulations were run at constant pressure[34] and temperature[35] with time constants of 1.0 ps and 0.1 ps for the pressure and temperature coupling, respectively. The LINCS algorithm was used to constrain bond lengths[36], allowing a time step of 2 fs in the classical simulations. SETTLE was applied to constrain the internal degrees of freedom of the water molecules. A 1.0 nm cut-off method was used for non-bonded Van der Waals' interactions, which were modeled by Lennard-Jones potentials. Coulomb interactions were computed with the smooth particle mesh Ewald method[37] using a 1.0 nm real space cut-off and a grid spacing of 0.12 nm. The relative tolerance of the real space cut-off was set to 10^{-5}. All simulations were performed in double precision with the Gromacs-4.5.4 molecular dynamics program.[38]

After equilibration, the simulation was continued for 5 ns in the NVE ensemble by switching off both temperature and pressure coupling. Only water molecules were constrained using SETTLE, while no constraints were used for the protein or micelle. The time step was reduced to 0.25 fs. Real-space cut-offs were shifted after 0.9 nm and the PME grid spacing was reduced to 0.11 and the relative tolerance was set to 10^{-6}. From the 5 ns NVE trajectory snapshots were taken every 100 ps to serve as starting points for the heat-transfer simulations.

To model the effect of the multi-photon absorption by the bacteriochlorophyll B co-factors, we assigned new velocities to the co-factor atoms. These velocities were randomly chosen from a Maxwell-Boltzmann distribution at an elevated temperature. This temperature was calculated under the assumption that all photons are converted into kinetic energy:

$$T_i^0 = m_i \frac{h\nu_i}{3k_B N_i}$$

where i identifies the cofactor (special pair or one of the auxiliary bacteriochlorophylls), N_i the number of atoms in the co-factor, ν_i the absorption frequency of co-factor i taken from

Breton et al.[39], k_B the Boltzmann constant and m_i the number of photons absorbed by cofactor *i*. For MD simulations we assumed that the special pair and the two auxiliary bacteriochlorophylls absorb 100 photons each. Although other cofactors may have absorbed some photon energy, this assumption is not considered to be severely limiting for this analysis since the energy rapidly flows out of the superheated cofactors into the protein (**Fig. 5a**), and the MD trajectories provide a large number of structures used for structural fitting. After assigning the new velocities to the co-factor atoms, the simulations were continued from the snapshots.

To monitor the flow of heat the system was divided into four subsystems: cofactors, protein, micelle and solvent. Excess heat $Q_i(t)$ in subsystem *i* was defined as the difference between total kinetic energy in these subsystems after multiple photon absorption and the average total kinetic energy in these systems in the equilibrium simulation at 300 K:

$$Q_i(t) = E_i^{kin}(t) - \langle E_i^{kin} \rangle_{T=300K}$$

Excess heat curves (**Fig. 3**) were obtained by averaging $Q_i(t)$ over 38 simulations. The temperature of the total system is not conserved with time (**Fig. 1a**) since some energy initially deposited into the cofactors is converted into potential energy within the system.

Structural refinement

Structural refinements against the C1 (ultrafast) and C2 (protein) basis spectra (**Fig. 1d**) were performed by χ^2 fitting of WAXS difference spectra using the error weighted χ^2 scoring function described in Malmerberg et al..[11] WAXS difference spectra were calculated from the set of pdb structures generated from MD simulations. 1000 pdb snapshots were extracted at 100 fs intervals from each of 36 photo-excited and 36 reference MD trajectories. X-ray scattering calculations compared MD trajectories of photo-excited structures (energy

deposited into the bacteriochlorophyll cofactors at $t = 0$ ps) against reference structures (no energy deposited) for which the paired trajectories both started from the same initial structure. Difference WAXS spectra, $\Delta S_{theory}(q)$, were calculated using the Debye formula and evaluated for their agreement with the C1 and C2 basis spectra using χ^2 scoring. Theoretical fits (**Fig. 3a** and **3b**) represent an average of the best 20 predictions for each of 36 trajectories: an ensemble average prediction from 720 structural pairs in total. Ensemble averaging was used since one should not visualize the laser pump as causing a light-induced shift from one static structure to another. Instead, dynamical motions occur within the protein on the picosecond time-scale that are larger than the light-induced perturbation to the ensemble average and it is a shift in the average distribution of an ensemble that is probed by TR-WAXS.

For structural fitting of C1 (the ultrafast component) only movements of the atoms of the bacteriochlorophyll cofactors were considered: specifically the atomic positions of these cofactors were extracted from the photoexcited and reference MD trajectories but all other atoms were frozen at their t = 0 conformation when calculating $\Delta S_{theory}(q)$. The resulting ensemble fit (**Fig. 3a**) supports our hypothesis that this component stems from ultrafast laser induced heating of the cofactors. For structural fitting of C2 (the protein component) all protein and cofactor atoms were allowed to move: specifically the atomic positions of all atoms were extracted from the photoexcited and reference MD trajectories when calculating $\Delta S_{theory}(q)$. The resulting ensemble fit (**Fig. 3b**) supports our hypothesis that the C2 component reflects an ultrafast global conformational change in RC$_{vir}$. Since the ratio of observations to variables is not favorable in TR-WAXS, these solutions are consistent with the data but are not necessarily unique since it cannot be ruled out that other conformations not sampled in our MD trajectories might yield analogous agreement to the TR-WAXS data.

Corrections to the WAXS patterns due to the presence of a detergent micelle and the excluded solvent volume were performed using the same assumptions as described when fitting time resolved WAXS spectra of bacteriorhodopsin and proteorhodopsin.[8,11] In particular, the dynamics of the detergent micelle were not modeled *per se*, but rather an average scattering detergent micelle correction was extracted from the reference trajectory and this correction was applied to both the photoexcited and referenced $\Delta S(q)$ calculations. Although this proved to be a critical assumption for structural refinement, since it avoided the fitting routine becoming dominated by movements of the detergent molecules within the micelle, the limitations of this assumption may contribute in part to a discrepancy between $\Delta S_{theory}(q)$ and $\Delta S_{experiment}(q)$ for $q \leq 0.2$ Å^{-1}. Fluctuations in the microjet, which causes stronger scattering at low q, also contributed experimental error in this domain.

No two pair of structures (photoexcited versus reference) selected by χ^2 fitting against the C2 basis spectrum gave identical structural changes. Recurring structural changes were identified by accepting that although all parts of the protein vary during MD simulations, the underlying global structural change should be present (at least to some extent) within all of the best pairs identified by χ^2 analysis. To extract these recurring structural changes from the ensemble of 900 best fits (the best 50 pairs from 18 paired MD trajectories of photoexcited and reference RC$_{vir}$) we first calculated a matrix $[\Delta C_\alpha]_{ij}$ of the change in the internal distances between C_α atoms ($[\Delta C_\alpha]_{ij} = [C_\alpha^{photoexcited} - C_\alpha^{reference}]_{ij}$, where i,j label all C_α atoms of RC$_{vir}$). We then determined the average, $Avg([\Delta C_\alpha]_{ij})$, and the standard deviation, $[\sigma(\Delta C_\alpha)]_{ij}$, of this ensemble set of 900 matrices. Finally we applied thresholds for which a movement was characterized as recurrent, requiring that the magnitude of the average internal distance matrix change was at least 90 % of the standard deviation of this change, $Avg([\Delta C_\alpha]_{ij}) \geq 0.9 \times [\sigma(\Delta C_\alpha)]_{ij}$, and that each selected C_α atom has at least 20 internal distance changes above this threshold. These C_α

atoms and the sign of their movements are highlighted graphically (**Fig. 3c**, **Supplementary Video 1**). Two striking features emerge from this analysis: only movements of two C_α atoms away from each other (*ie*. $Avg([\Delta \mathbf{C}_\alpha]_{ij}) \geq 0$, orange spheres in **Fig. 3c**) were identified as recurrent, with no case being identified for which two C_α atoms moved towards each other passing these thresholds; and almost all C_α atoms identified in this manner were associated with the TM domains of subunits H, L and M (**Fig. 3c**).

ONLINE REFERENCES:

21   DePonte, D. P. *et al.* Gas dynamic virtual nozzle for generation of microscopic droplet streams. *J. Phys. D Appl. Phys.* **41**, 195505 (2008).

22   Hart, P. *et al.* The CSPAD megapixel x-ray camera at LCLS. *Proc. SPIE* **8504**, 85040C (2012).

23   Georgiou, P. *et al.* Picosecond calorimetry: Time-resolved X-ray diffraction studies of liquid CH_2Cl_2. *J. Chem. Biol.* **124**, 234507 (2006).

24   Clayton, R. K. & Clayton, B. J. Molar extinction coefficients and other properties of an improved reaction center preparation from *Rhodopseudomonas viridis. Biochim. Biophys. Acta* **501**, 478-487 (1978).

25   Valkunas, L. & Gulbinas, V. Nonlinear exciton annihilation and local heating effects in photosynthetic antenna systems. *Photochem. Photobiol.* **66**, 628-634 (1997).

26   Valkunas, L., Trinkunas, G., Liuolia, V. & van Grondelle, R. Nonlinear annihilation of excitations in photosynthetic systems. *Biophys. J.* **69**, 1117-1129 (1995).

27   Kasha, M. Characterization of Electronic Transitions in Complex Molecules. *Disc. Faraday Soc.* **9**, 14-19 (1950).

28   Cammarata, M. *et al.* Chopper system for time resolved experiments with synchrotron radiation. *Rev. Sci. Instrum.* **80**, 015101 (2009).

29   Deisenhofer, J., Epp, O., Sinning, I. & Michel, H. Crystallographic refinement at 2.3 Å resolution and refined model of the photosynthetic reaction centre from Rhodopseudomonas viridis. *J. Mol. Biol.* **246**, 429-457 (1995).

30   Duan, Y. *et al.* A point-charge force field for molecular mechanics simulations of proteins based on condensed-phase quantum mechanical calculations. *J. Comput. Chem.* **24**, 1999-2012 (2003).

31   Ceccarelli, M., Procacci, P. & Marchi, M. An ab initio force field for the cofactors of bacterial photosynthesis. *J. Comput. Chem.* **24**, 129-142 (2003).

32   Autenrieth, F., Tajkorsid, E., Baudry, J. & Luthey-Schulten, Z. Classical force field parameters for the heme prosthetic group of cytochrome c *J. Comput. Chem.* **25**, 1613-1622 (2004).

33   Gast, P., Hemelrijk, P. & Hoff, A. J. Determination of the number of detergent molecules associated with the reaction center protein isolated from the photosynthetic bacterium *Rhodopseudomonas viridis*. Effects of the amphiphilic molecule 1,2,3-heptanetriol. *FEBS Lett.* **337**, 39-42 (1994).

34   Berendsen, H. J. C., Postma, J. P. M., Van Gunsteren, W. F., Dinola, A. & Haak, J. R. Molecular-dynamics with coupling to an external bath. *J. Chem. Phys.* **81**, 3684-3690 (1984).

35   Bussi, G., Donadio, D. & Parrinello, M. Canonical sampling through velocity rescaling. *J. Chem. Phys.* **126**, 014101 (2007).

36   Hess, B., Bekker, H., Berendsen, H. J. C. & Fraaije, J. G. E. M. LINCS: A linear constraint solver for molecular simulations. *J. Comp. Chem.* **18**, 1463-1472 (1997).

37   Essmann, U. *et al.* A smooth particle mesh Ewald method. *J. Chem. Phys.* **103**, 8577-8593 (1995).

38   Hess, B., Kutzner, C., Van der Spoel, D. & Lindahl, E. GROMACS 4: Algorithms for highly efficient, load-balanced, and scalable molecular simulation. *J. Chem. Theo. Comp.* **4**, 435-447 (2007).

39   Breton, J., Martin, J. L., Migus, A., Antonetti, A. & Orszag, A. Femtosecond spectroscopy of excitation energy transfer and initial charge separation in the reaction center of the photosynthetic bacterium *Rhodopseudomonas viridis*. *Proc. Natl. Acad. Sci. USA* **83**, 5121-5125 (1986).
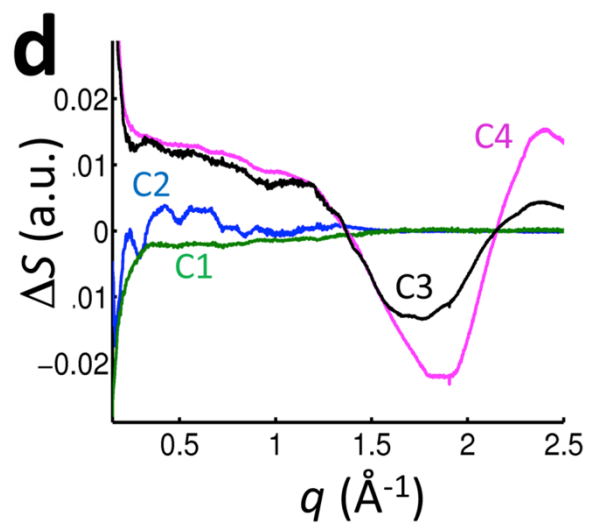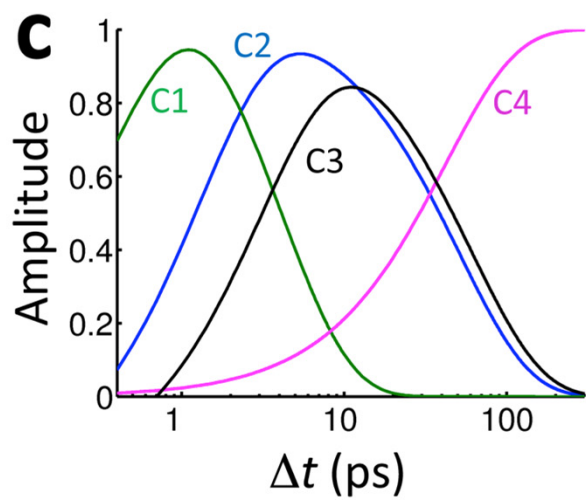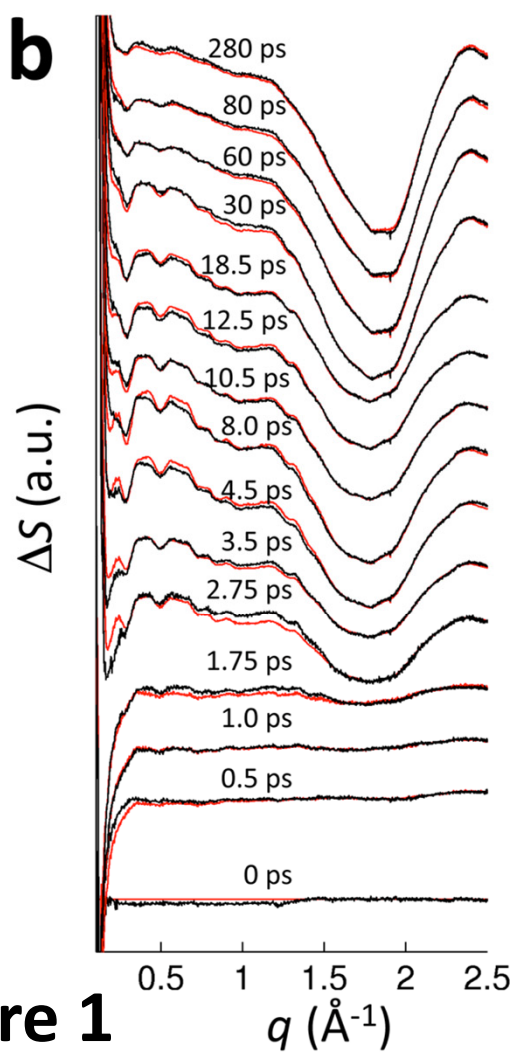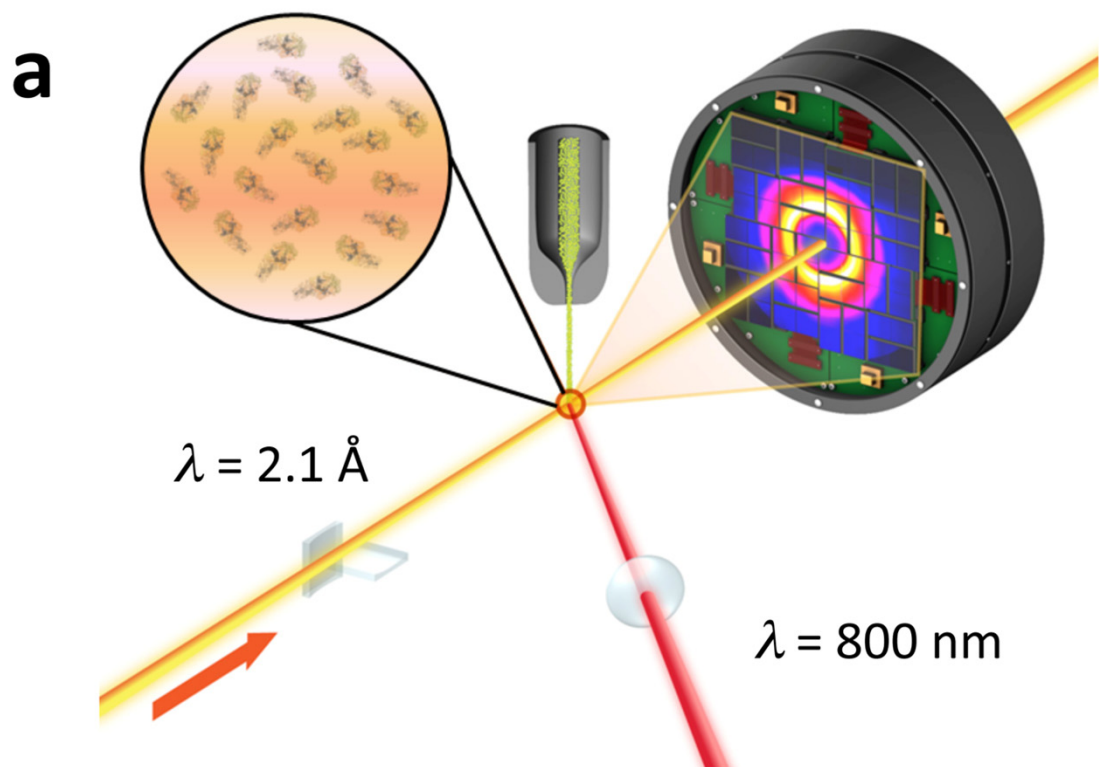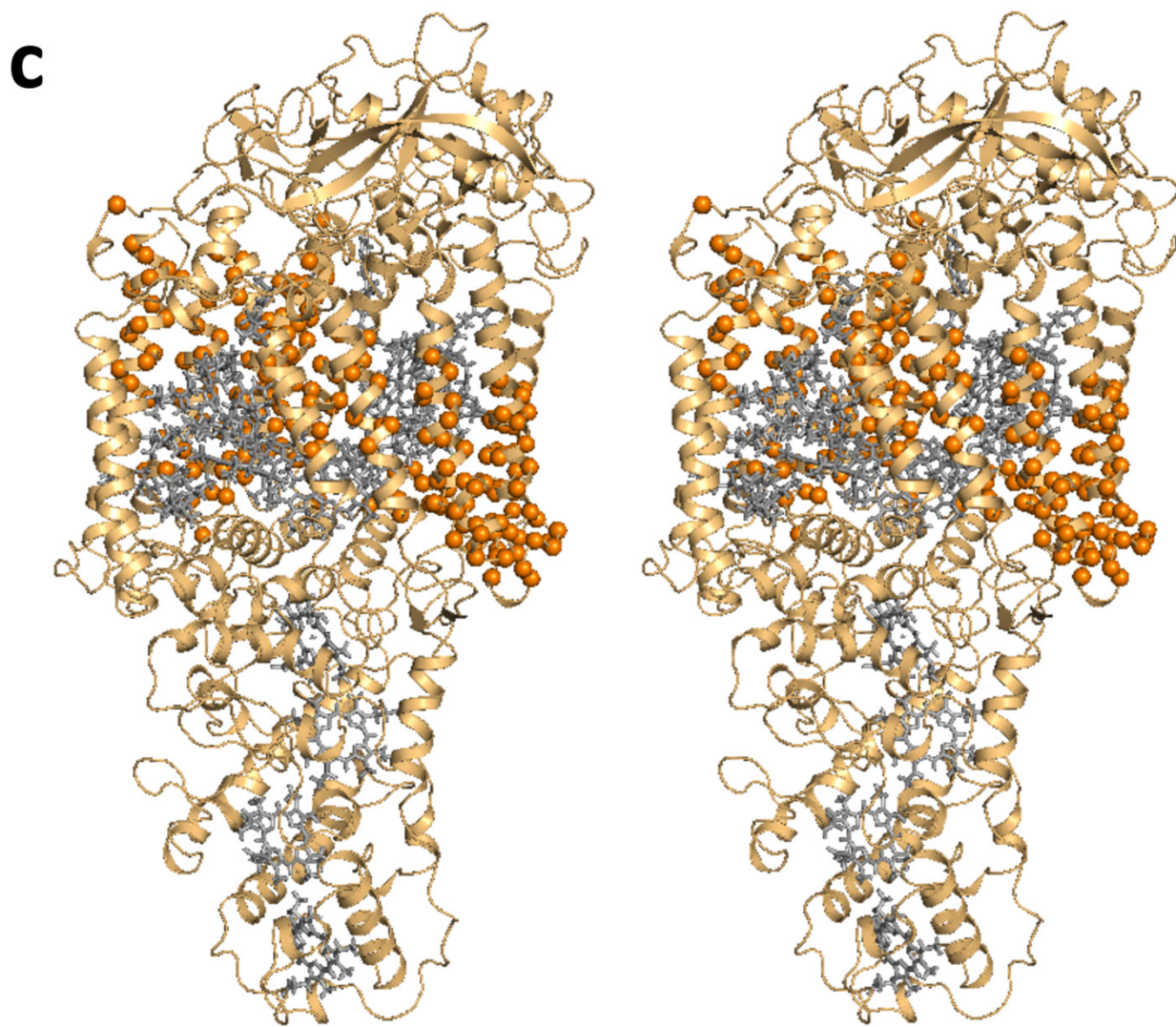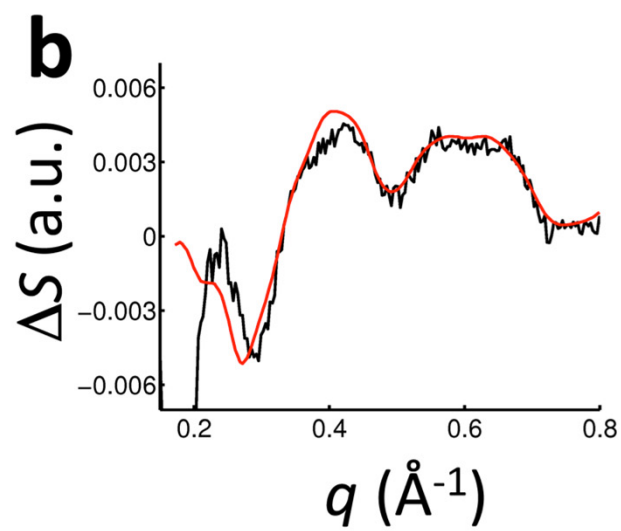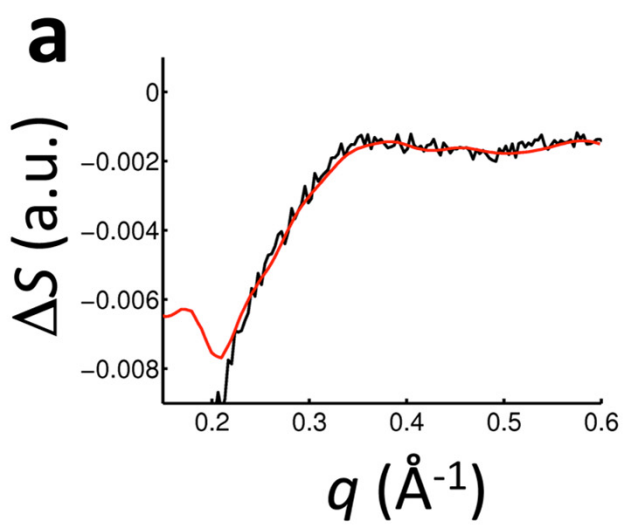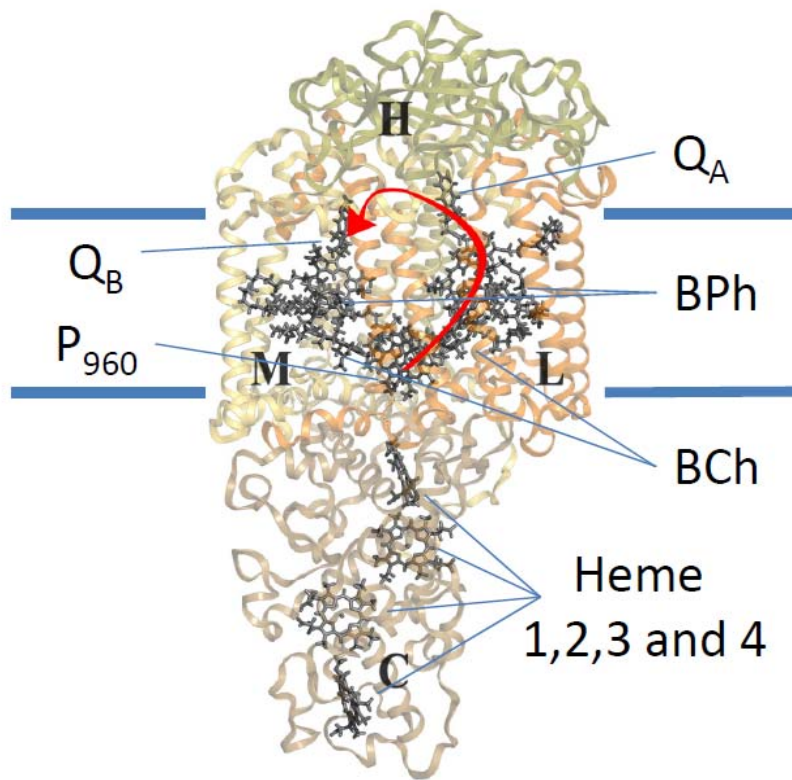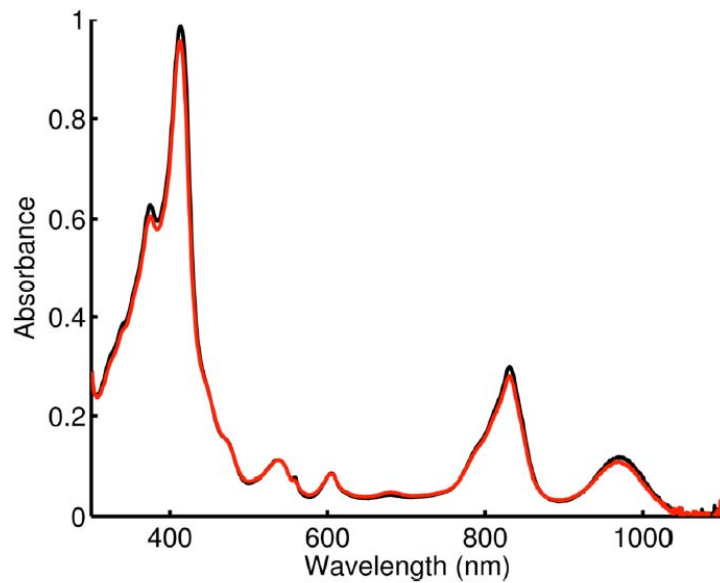
Figure 1
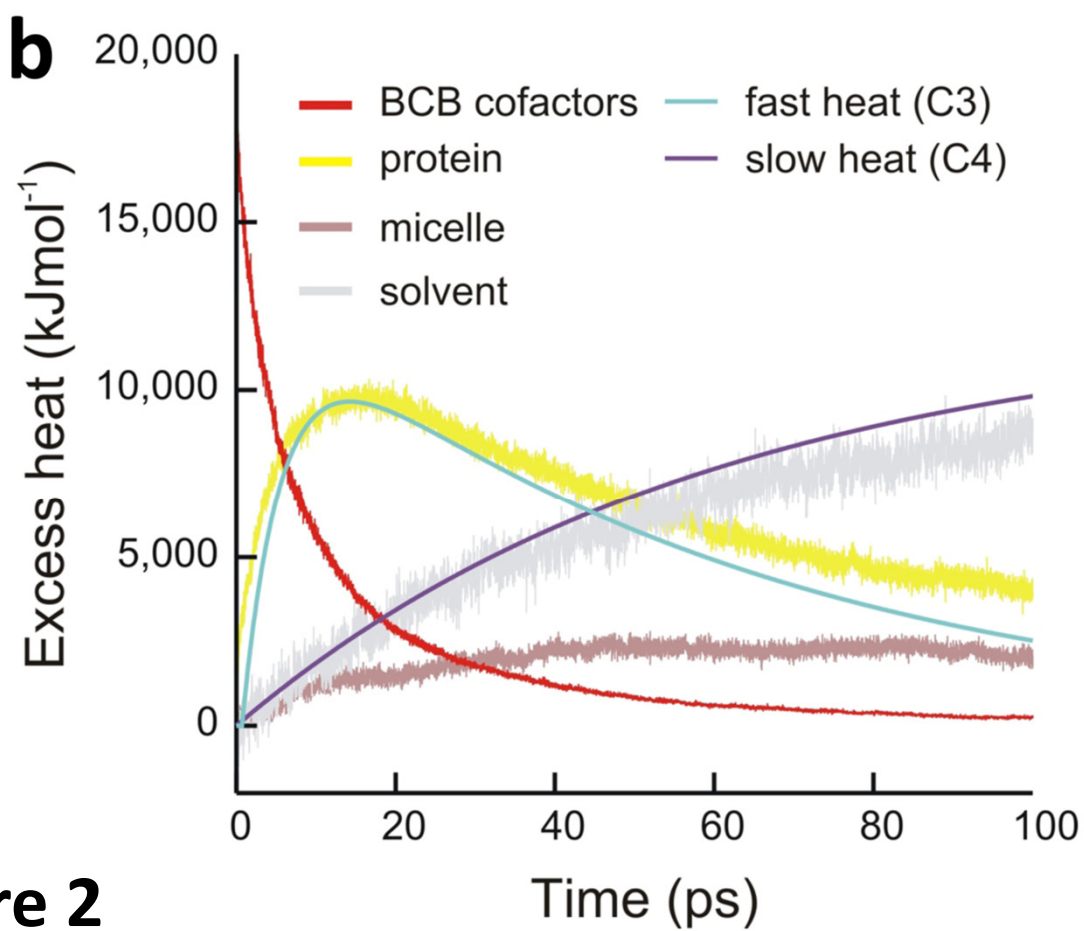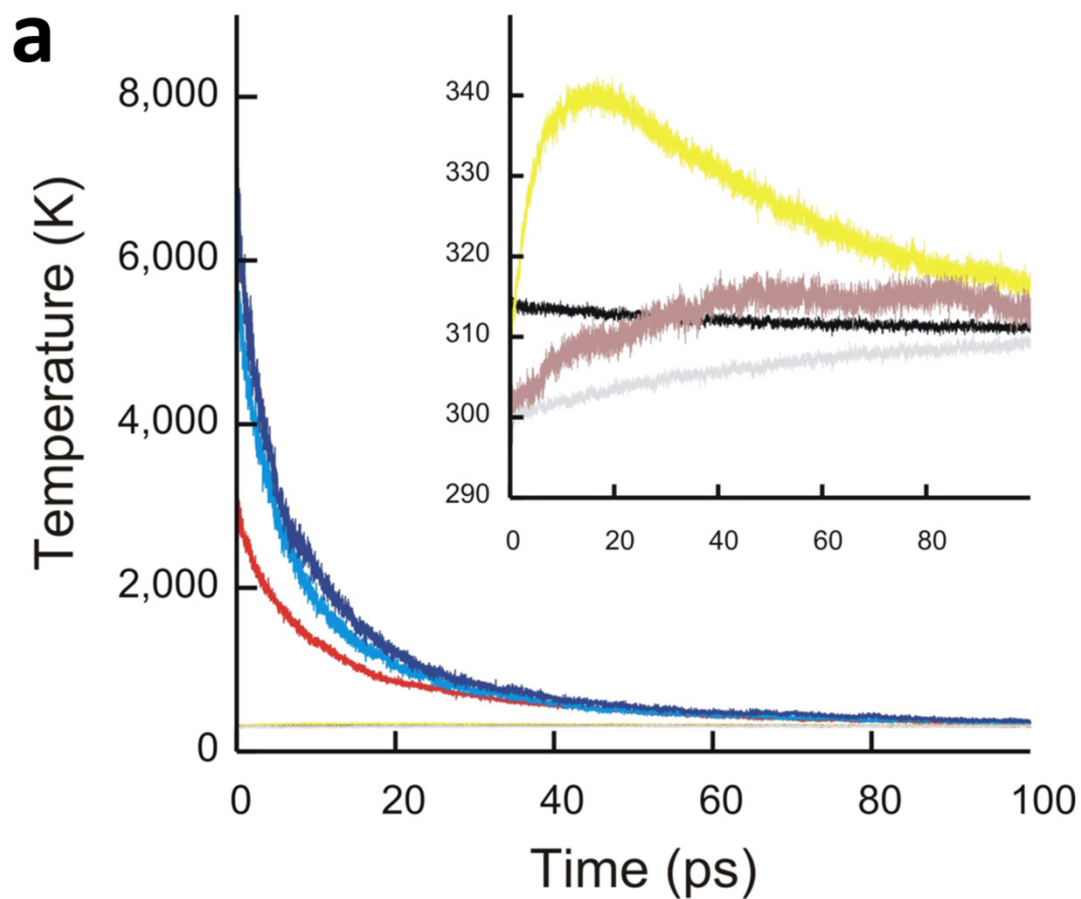
Figure 2

Figure 3

Supplementary Figure 1

**Structure of the *Bl. viridis* photosynthetic reaction center.**

RC$_{vir}$ consists of transmembrane subunits L and M that support a special pair of bacteriochlorophylls (P$_{960}$), two monomeric bacteriochlorophylls (BCh), two bacteriopheophytins molecules (BPh), a tightly bound menaquinone (Q$_A$) and a mobile quinone (Q$_B$) arranged around an axis of two-fold pseudo-symmetry. RC$_{vir}$ is capped from the cytoplasm by the H-subunit and from the periplasm by the tetraheme containing C-subunit. Photo-oxidation of P$_{960}$ causes an electron to move to Q$_B$ on the opposite side of the membrane (red arrow) whereupon P$_{960}^+$ is reduced from the heme groups of the C-subunit. A second photo-oxidation reaction causes the Q$_B^-$ semiquinone to be fully reduced to quinol, protonated from the cytoplasm and released into the membrane. Blue lines indicate approximate membrane boundaries. In this work multi-photon excitation was used, resulting in the rapid heating of the BCh cofactors and the single-photon electron transfer scheme above does not necessarily apply.

Supplementary Figure 2

Absorption spectra from detergent solubilized RC$_{vir}$ before and after exposure to a single 800 nm fs laser pulse.

RC$_{vir}$ samples were exposed to a pump laser of 500 fs in duration tuned to a fluence of 4.4 mJ mm^{-2} per pulse and operated at a repetition rate of 1 kHz. Samples were passed through a 300 μm quartz capillary and diluted to achieve OD$_{800\ nm}$ = 1 through this capillary. The capillary was placed in the focus of the fs laser beam. The rate of flow of the sample through the quartz capillary was chosen so that each and every sample volume was exposed once, and only once, to the 800 nm pulse. Samples were collected and steady-state spectra (shown) were taking after the sample was loaded into a 10 mm path length cuvette and diluted 200 fold. The red line shows absorption spectra recorded from samples exposed to the fs laser, whereas the black line corresponds to samples that were not exposed. These spectra are averaged over three repeats.
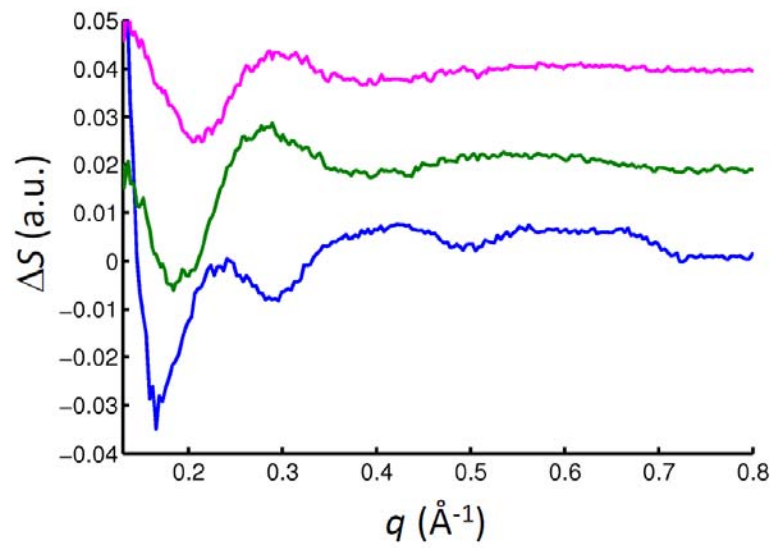
Supplementary Figure 3

Changes in WAXS difference spectra due to structural changes in membrane proteins.

Comparison of the protein difference WAXS basis spectrum for RC_{vir} (C2 of **Fig. 1b**, blue) with two basis spectra recorded using TR-WAXS studies of bacteriorhodopsin (bR): magenta, the basis spectrum arising from bR with a time-constant of 22 μs; green the basis spectrum arising from bR with a time-constant of 1.9 ms; blue, the basis spectrum arising from RC_{vir} with a half rise of 1.4 ps. The two bR basis spectra have been arbitrarily scaled to assist comparison with the RC_{vir} basis spectrum.
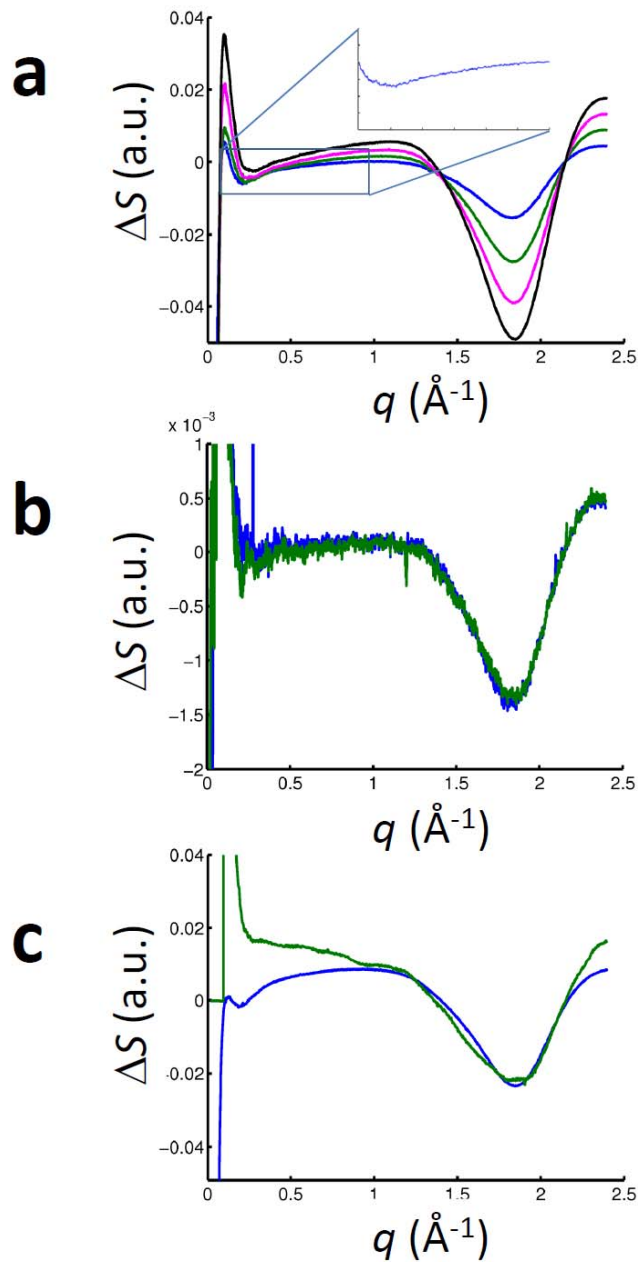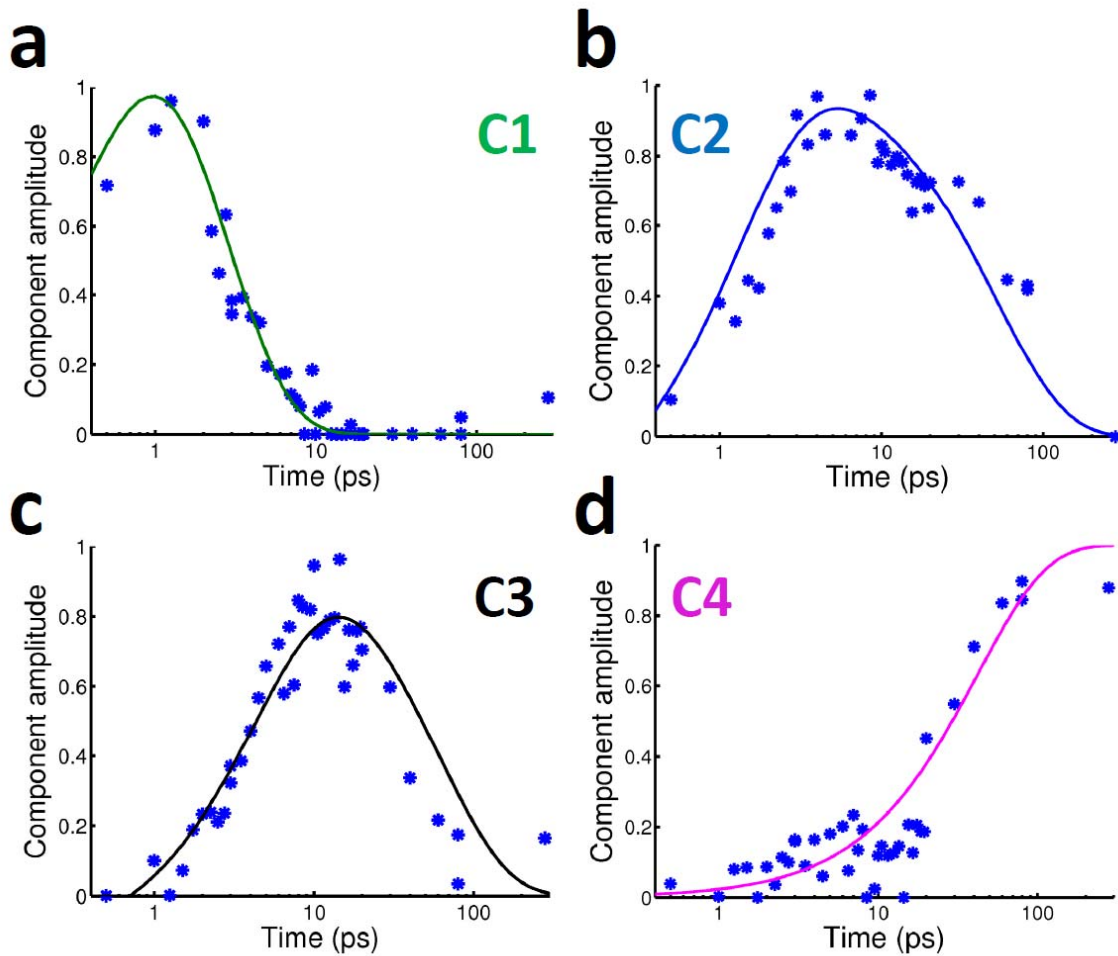
Supplementary Figure 4

Changes in WAXS spectra from detergent solubilized RC$_{vir}$ due to heating.

(**a**) Temperature dependence of $\Delta S(q)$ measured by continuously heating the sample when held in a capillary at a synchrotron radiation source. The inset (0.2 Å^{-1} ≤ q ≤ 0.8 Å^{-1}) illustrates that the oscillatory features observed in ultrafast time-resolved WAXS data (**Fig. 1**) do not arise when continuously heating the sample. The temperature changes used for these measurements were 5 ºC (blue; also inset); 10 ºC (green); 15 ºC (magenta) and 20 ºC (light blue). (**b**) Measurements of $\Delta S(q,\Delta t)$ recorded using 100 ps X-ray pulses of synchrotron radiation for the time delays Δt = 280 ps and Δt = 1 μs. (**c**) Overlay of the $\Delta S(q, \Delta t$ = 280 ps) from XFEL data (green) with $\Delta S(q)$ corresponding to a 7 ºC temperature change (blue). The blue curve was recovered by interpolating the data in **a** and simulating random fluctuations in the background associated with XFEL data (Online Methods).
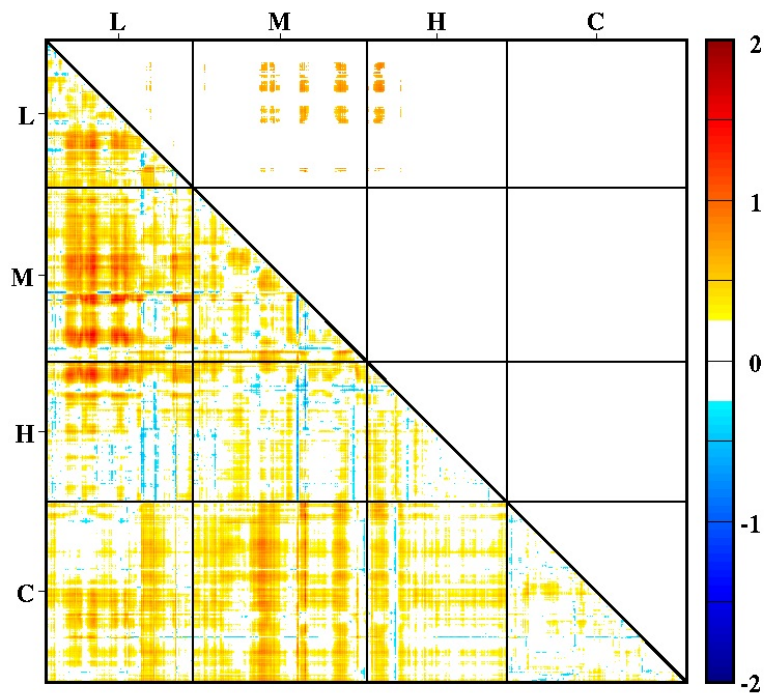
Supplementary Figure 5

Time-dependent linear amplitudes of the WAXS basis spectra extracted by spectral decomposition.

(**a**) Time dependence of the ultrafast (C1) component. (**b**) Time dependence of the protein (C2) component. (**c**) Time dependence of the non-equilibrated heating (C3) component. (**d**) Time dependence of the equilibrated heating (C4) component. Linear amplitudes of these components are shown as blue stars and the time dependent amplitudes used for spectral decomposition are shown as continuous lines. Colors chosen to be consistent with **Fig. 1**.

Supplementary Figure 6

Recurring movements extracted from an ensemble average approach to structural fitting against the experimental C2 basis spectrum.

Bottom left: Matrix representation of the average internal distance changes calculated on C_α atoms, $\mathrm{Avg}([\Delta \mathbf{C}_\alpha]_{ij})$, divided by the standard deviation of these changes, $[\sigma(\Delta \mathbf{C}_\alpha)]_{ij}$. This matrix was calculated from an ensemble of 900 best fits identified by χ^2 minimization against the protein difference WAXS component C2. **Top right**: Recurring movements, defined as $\mathrm{Avg}([\Delta \mathbf{C}_\alpha]_{ij}) \geq 0.9 \times [\sigma(\Delta \mathbf{C}_\alpha)]_{ij}$ relative to at least 20 other C_a atoms (Online Methods). Only changes corresponding to movements of C_α atoms away from each other ($[\Delta \mathbf{C}_\alpha]_{ij} > 0$) were classified as recurring, with no inwards movements ($[\Delta \mathbf{C}_\alpha]_{ij} < 0$) noted above this threshold. All of these movements are associated with the TM helices of subunits H, L and M and are represented as orange spheres on the atomic coordinates in **Fig. 3C**.